

# ARTIFICIAL NEURAL NETWORKS APPLIED TO SINGLE-PHASE LOAD HARMONIC CHARACTERIZATION

Claudionor F. Nascimento<sup>\*</sup>, Azauri A. Oliveira Jr.<sup>†</sup>, Alessandro Goedtel<sup>‡</sup>,  
Marcelo Suetake<sup>†</sup>, Ivan N. Silva<sup>†</sup>

<sup>\*</sup>Federal University of ABC, Santo André SP, Brazil

<sup>†</sup>University of São Paulo, São Carlos SP, Brazil

<sup>‡</sup>Federal University of Technology - Paraná, Cornélio Procópio PR, Brazil

claudionor.nascimento@ufabc.edu.br, {azaaurijr, mclsuetake, insilva}@sel.eesc.usp.br, agoedtel@utfpr.edu.br

**Abstract** – In this paper, an alternative method based on artificial neural networks is presented for the determination of load current harmonic components in a single-phase electric power system. The first six harmonic components are calculated from current waveforms of an AC controller and a single-phase diode bridge rectifier, which are the most common loads in industrial, commercial and residential applications. The influences of such nonlinear loads in power quality issues are also characterized. The proposed method is compared with truncated FFT. Simulation and experimental results are presented in order to validate the proposed approach.

**Keywords** - Artificial neural networks, harmonic identification, power quality, single-phase power system.

## I. INTRODUCTION

The use of devices and equipments based on static converter has been in constant growing which awakes the attention to several problems such that nonlinear loads cause in the Power Quality (PQ). In [1], it is showed that the PQ can be evaluated by using an Artificial Neural Network (ANN).

Such loads produce perturbations to the electric power system and, consequently, results in a decreasing PQ. In large quantities, nonlinear single-phase loads can cause a great harmonic distortion in industrial, residential and commercial environments [2], [3].

The determination of harmonic contents aims to characterize nonlinear load behaviors [3]-[5] and quantify the harmonic distortions. It also can be used in a system that compensates such distortions [6]-[10]. The harmonic contents can be calculated by two approaches: in time-domain [6] and in frequency-domain [9]. The latter uses the traditional techniques for signal spectral analysis such as Fourier series and discrete Fourier transform [3]. As alternative methods, some previous works have presented an application of ANN to determine the harmonic contents in three-phase and single-phase electric power system [7], [10].

The ANNs are widely used in power electronic issues [11]-[13], including in hardware applications such as Digital Signal Processor (DSP) and Field-Programmable Gate Array (FPGA) [14], [15].

Several kinds of loads present a well-known theoretical behavior, e.g., a typical diode rectifier that interfaces the AC-DC conversions between an AC power supply and a switching power supply [4].

However, some loads are subjected to waveform variations and can lead to uncertainties in their current waveforms. This problem can increase the computational cost when conventional methods are used for active compensation.

In this article, an alternative method based on ANN with offline training is proposed to estimate the  $A_n$  and  $B_n$  Fourier series coefficients of single-phase current drained simultaneously by commercial AC controller (dimmer) and diode bridge rectifier. The harmonic components are online identified during a half-cycle of voltage supply waveform. The use of  $A_n$  and  $B_n$  allows the identification of amplitude and phase angle components of a distorted signal.

This paper is organized as follow: In Section II, the characteristics of loads used in this work are presented. In Section III, the principles of ANN and the experimental results of  $A_n$  e  $B_n$  Fourier series coefficient estimation of load current are reported. Finally, the conclusions of this work are described in Section IV.

## II. NONLINEAR LOADS

The dimmer and the diode bridge rectifier are illustrated in Fig. 1. They represent nonlinear loads for the sinusoidal voltage source ( $v_s(t)$ ). When only  $S_1$  is closed, then  $i_s(t) = i_{L2}(t)$ . On the other hand, when only  $S_2$  is closed, then  $i_s(t) = i_{L1}(t)$ . When both  $S_1$  and  $S_2$  are closed, then  $i_s(t) = i_{L1}(t) + i_{L2}(t)$ .

This load is composed of power electronic semiconductor switches. The current waveform of this system changes both with firing angle  $\alpha'$  of dimmer main component (*TRIAC A*) and the resistance  $R_L$  of lamps sets, which also changes with temperature.

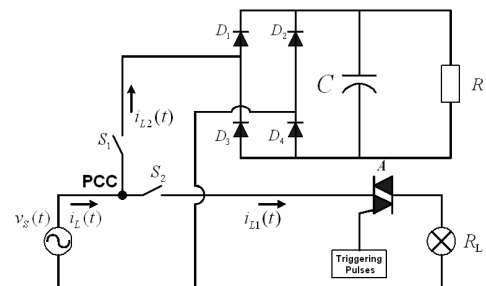


Fig. 1. Dimmer and rectifier system.

In current waveform analysis, the Fourier series was used as showed in (1), where  $f_0$  is the fundamental frequency [16].

$$x(t) = \sum_{n=1}^{\infty} A_n \cos(2\pi n f_0 t) + B_n \sin(2\pi n f_0 t) \quad (1)$$

The  $A_n$  and  $B_n$  ( $n = 1, 2, 3, \dots$ ) Fourier series coefficients can be calculated, in  $T_0$  period, by:

$$A_n = \frac{2}{T_0} \int_{-T_0/2}^{T_0/2} x(t) \cos(2\pi n f_0 t) dt \quad (2)$$

$$B_n = \frac{2}{T_0} \int_{-T_0/2}^{T_0/2} x(t) \sin(2\pi n f_0 t) dt \quad (3)$$

In the vector form, (2) and (3) can be re-written as:

$$c_n \angle \theta_n = A_n + jB_n \quad (4)$$

where its amplitude and phase angle are given by:

$$c_n = \sqrt{A_n^2 + B_n^2} \quad (5)$$

$$\phi_n = \tan^{-1} \left( \frac{A_n}{B_n} \right) \quad (6)$$

Therefore, the Fourier series is represented as follow:

$$x(t) = \sum_{n=1}^{\infty} c_n \sin(2\pi n f_0 t + \phi_n) \quad (7)$$

The current waveform Fourier series (for  $n = 3, 5, \dots$ ) of the dimmer is illustrated in Fig. 2(a), where  $S_1$  switch open and  $S_2$  switch closed, is described in (8). The symbol  $V$  is the voltage peak.

$$i_{L1}(t) = \frac{V}{\pi R_L} \left\{ \frac{1}{2} [\cos 2\alpha' - 1] \cos \omega t + \frac{1}{2} [\sin 2\alpha' + 2\pi - 2\alpha'] \sin \omega t + \sum_{n=3}^{\infty} \left[ \frac{\cos(n+1)\alpha' - \cos(n+1)\pi}{n+1} - \frac{\cos(n-1)\alpha' - \cos(n-1)\pi}{n-1} \right] \cos n\omega t + \sum_{n=3}^{\infty} \left[ \frac{\sin(n+1)\alpha'}{n+1} - \frac{\sin(n-1)\alpha'}{n-1} \right] \sin n\omega t \right\} \quad (8)$$

The current waveform Fourier series (for  $n = 3, 5, \dots$ ) of diode bridge rectifier illustrated in Fig. 2(b), where  $S_1$  switch closed and  $S_2$  switch open, is described in (9).

$$i_{L2}(t) = \frac{2}{\pi} \left\{ \left[ \frac{k_0}{k_s^2 + 1} [e^{-k_s \beta} [-k_s \cos(\beta) - \sin(\beta)] - e^{-k_s \alpha} [-k_s \cos(\alpha) - \sin(\alpha)]] + \frac{k_3}{4} [\cos(2\alpha) - \cos(2\beta)] + \frac{k_4}{4} [\sin(2\beta) - \sin(2\alpha) + 2\beta - 2\alpha] \right] \cos(\omega t) + \left[ \frac{k_0}{k_s^2 + 1} [e^{-k_s \beta} [-k_s \sin(\beta) - \cos(\beta)] - e^{-k_s \alpha} [-k_s \sin(\alpha) - \cos(\alpha)]] + \frac{k_4}{4} [\cos(2\alpha) - \cos(2\beta)] + \frac{k_3}{4} [\sin(2\alpha) - \sin(2\beta) + 2\beta - 2\alpha] \right] \sin(\omega t) + \sum_{n=3}^{\infty} \left[ \frac{k_0}{k_s^2 + n^2} [e^{-k_s \beta} [-k_s \cos(n\beta) - n \sin(n\beta)] - e^{-k_s \alpha} [-k_s \cos(n\alpha) - n \sin(n\alpha)]] + \frac{k_3}{2} \left( \frac{\cos(n+1)\alpha - \cos(n+1)\beta}{(n+1)} + \frac{\cos(n-1)\beta - \cos(n-1)\alpha}{(n-1)} \right) + \frac{k_4}{2} \left( \frac{\sin(n+1)\beta - \sin(n+1)\alpha}{(n+1)} + \frac{\sin(n-1)\beta - \sin(n-1)\alpha}{(n-1)} \right) \right] \cos(n\omega t) + \sum_{n=3}^{\infty} \left[ \frac{k_0}{k_s^2 + n^2} [e^{-k_s \beta} [-k_s \sin(n\beta) - n \cos(n\beta)] - e^{-k_s \alpha} [-k_s \sin(n\alpha) - n \cos(n\alpha)]] + \frac{k_4}{2} \left( \frac{\cos(n+1)\alpha - \cos(n+1)\beta}{(n+1)} + \frac{\cos(n-1)\alpha - \cos(n-1)\beta}{(n-1)} \right) + \frac{k_3}{2} \left( \frac{\sin(n+1)\alpha - \sin(n+1)\beta}{(n+1)} + \frac{\sin(n-1)\beta - \sin(n-1)\alpha}{(n-1)} \right) \right] \sin(n\omega t) \right\} \quad (9)$$

where  $\alpha$  is the start  $\beta$  is the end of diode conductions, and:

$$k_0 = e^{-k_s t_0} [k_3 \sin(\omega t_0) + k_4 \cos(\omega t_0)] \quad (10)$$

$$k_1 = \frac{1}{C} \left( \frac{1}{R_2} + \frac{1}{R} \right) \quad (11)$$

$$k_2 = \frac{V}{R_2 C} \quad (12)$$

$$k_3 = \frac{1}{R_2} \left( V - \frac{k_1 k_2}{k_1^2 + \omega^2} \right) \quad (13)$$

$$k_4 = \frac{1}{R_2} \left( \frac{\omega k_2}{k_1^2 + \omega^2} \right) \quad (14)$$

$$k_5 = \left( \frac{k_1}{\omega} \right) \quad (15)$$

Fig. 2(b) shows the current waveform of diode bridge rectifier. It is relevant to mention that the load coefficients are constant because the resistor  $R$  and the capacitor  $C$  have also constant values.

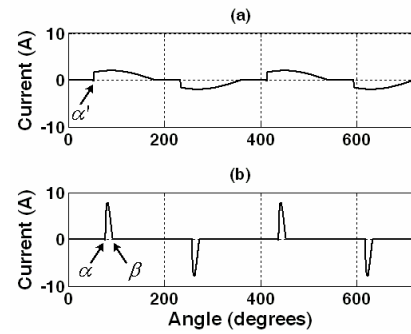


Fig. 2. Dimmer current (a) and rectifier current (b) (simulation).

The theoretical variation of  $A_n$  and  $B_n$  coefficients of total current (dimmer current and diode bridge rectifier current) at Point of Common Coupling (PCC) in function of dimmer firing angle is illustrated in Fig. 3 and 4. Notice that this is the case where  $S_1$  and  $S_2$  are both closed.

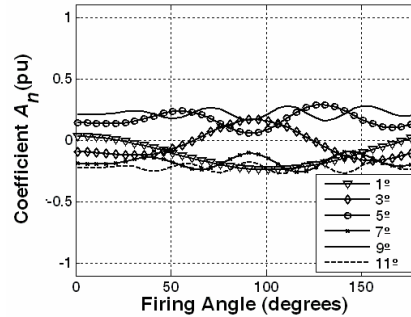


Fig. 3.  $A_n$  coefficient of current (simulation).

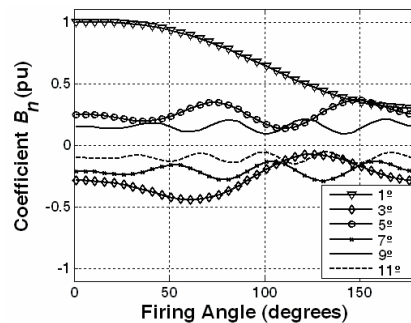


Fig. 4.  $B_n$  coefficient of current (simulation).

Fig. 5 shows the nonlinear variation of RMS current ( $I_{RMS}$ ) of dimmer and diode bridge rectifier at PCC. It can be calculated using the  $n$ -th harmonic component of current as follow:

$$I_{RMS} = \sqrt{\sum_{n=1}^N \frac{I_n^2}{2}} \quad (16)$$

The Total Harmonic Distortion (*THD*) of current is given by (17) [17].

$$THD = \frac{\sqrt{\sum_{n=2}^{\infty} I_n^2}}{I_1} \quad (17)$$

Fig. 5 illustrates the *THD* current variation in function of dimmer firing angle, considering the case of both load are switched on. It is verified that the *THD* reaches 251% for firing angle close to 180° due to the predominant amplitudes of diode bridge rectifier over dimmer.

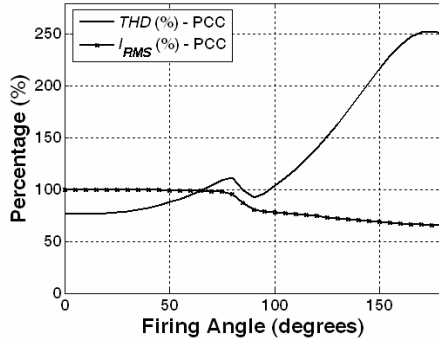


Fig. 5. Variation of RMS and *THD* current (simulation).

In order to calculate the real Power Factor (*PF*) of the system connected with nonlinear loads, the *THD* influences have to be taken into account. In a system where nonlinear loads are present, the cosine angle of the angle between fundamental voltage and fundamental current ( $\cos\theta_1$ ) is defined as Displacement Factor (*DF*). The *THD*, which is quantified to a system Distortion Factor (*Dist.F*), is responsible for changing the *PF* where only fundamental quantities are considered. Therefore the real *PF* of the system can be calculated as follow [2]:

$$PF = (Dist.F)(DF) = \frac{1}{\sqrt{1+(THD)^2}} \cos\theta_1 \quad (18)$$

The low *PF* together with high harmonic distortion can cause some problems such as limitation of maximum power supply [2].

The featured behavior of fundamental component and first five harmonic components of load current (dimmer and diode bridge rectifier) is shown in Fig. 6.

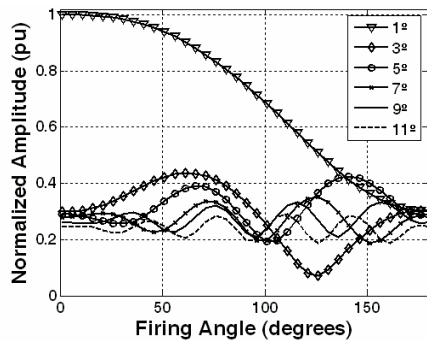


Fig. 6. Current amplitude variations at PCC (simulation).

Fig. 7 illustrates the *PF* of nonlinear loads. The diode bridge rectifier *PF* is low and constant (0.3677) whereas the dimmer *PF* initially has a unitary value (resistive load) and decreases with the increasing of firing angle. The curve that represents the *PF* at PCC has a variation at the same firing angle of *THD*, starting from around 0.8 and getting constant when it reaches the diode bridge rectifier, though.

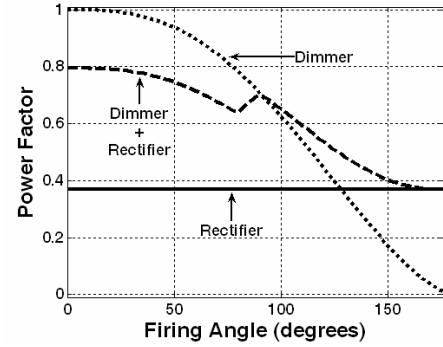


Fig. 7. Load *PF* Variation (Simulation).

### III. HARMONIC IDENTIFICATION

#### A. Artificial Neural Networks Application

The basic architecture for the determination of harmonic contents by ANN is illustrated in Fig. 8. A set of 42 samples with current amplitude is acquired within a half-cycle of voltage supply waveform (5.04 kHz sample rate). Therefore, a Multilayer Perceptron (MLP) neural network, also composed of 42 inputs, will receive the respective current signal samples. The neural estimator structure was chosen by the cross-validation procedure [18], which is composed of 5 neurons in hidden layer and one neuron in output layer that provides one of the Fourier series coefficients. Therefore, there are 12 neural structures providing the  $A_n$  and  $B_n$  outputs ( $n = 1, 3, 5, 7, 9$  and  $11$ ).

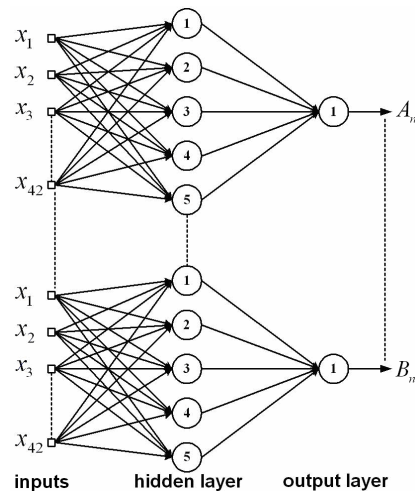


Fig. 8. The artificial neural network structure used for Fourier series coefficients estimation.

The database contains 101 vectors, where 90 of them (simulation data) are used for supervised training process and the remaining 11 vectors (experimental data) are used in ANN validation phase.

The synaptic weights of each artificial neuron are adjusted by a supervised training algorithm (Levenberg-Marquardt algorithm) so that the ANN approximates the input signals to the desired output. The activation function of each hidden layer neuron consists of hyperbolic tangent function whereas the output neuron is linear function.

The experimental database for ANN estimator training and validation was built through the test bench illustrated on Fig. 9. This structure is responsible to acquire voltages and

currents data of a commercial dimmer which feeds a set of three incandescent lamps of 100 W (220 V) each, a diode bridge rectifier with capacitor filter of 470  $\mu\text{F}$  and resistive load of 730  $\Omega$ . All data was acquired by the NI-DSQ USB 6009 data acquisition of National Instruments where Labview software was used for PC interfacing. The Hall sensor employed to measure currents and the firing angle limitations are detailed in [2]. Matlab/Simulink was used for simulation task and results presentations.

The AC voltage supply ( $v_s(t)$ ) and total load current ( $i_L(t) = i_{L1}(t) + i_{L2}(t)$ ) are presented in Fig. 10.

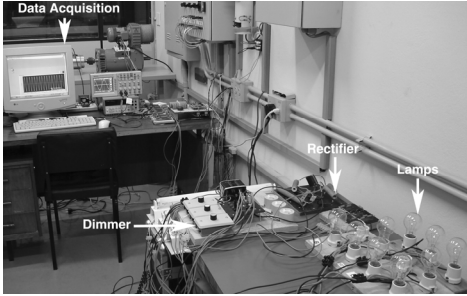


Fig. 9. Load structure built on test bench (experimental).

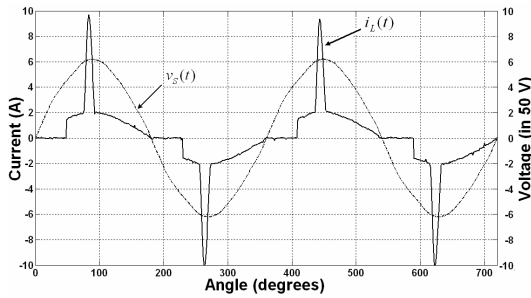


Fig. 10. Voltage supply and total load current (experimental).

The instantaneous current is therefore sampled from dimmer and diode bridge rectifier and then provided to the proposed ANN which estimates the harmonic component coefficients.

The results reported in Sections B and C show the comparison between the Fourier coefficients ( $A_n$  and  $B_n$ ) estimated from ANN and the respective target value. The total training time was 2.45 seconds, where minimum squared error of  $5.10^{-3}$  and 1000 training epochs were set for stop criterion. The ANN training process was achieved offline using a Pentium 4 (clock of 3 GHz) personal computer with 1 GB RAM memory.

### B. Experimental Results

Figs. 11 to 22 show the performance of the ANN based Fourier series estimator whereby it can be noticed that the proposed method was able to generalize solutions and map the behavior between the firing angle of a commercial dimmer (limited to  $22^\circ$  and  $130^\circ$  as a result of constructive aspects) and the Fourier series coefficients. Figs. 11 to 22 also show the behavior of 4 curves where two of them represent the estimated and the target value of load current of dimmer only. The other two curves represent the sum estimative results of load currents Fourier coefficients at PCC, that is, sums of dimmer and diode bridge rectifier current.

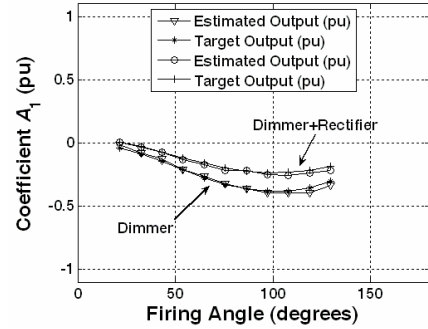


Fig. 11.  $A_1$  current coefficient (experimental).

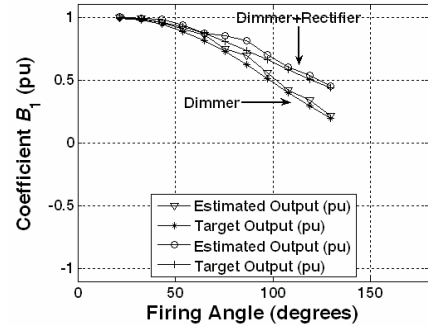


Fig. 12.  $B_1$  current coefficient (experimental).

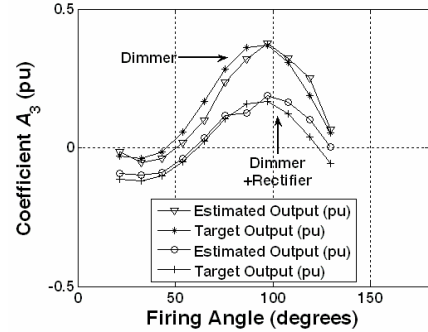


Fig. 13.  $A_3$  current coefficient (experimental).

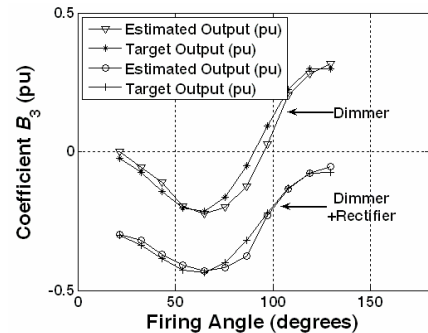


Fig. 14.  $B_3$  current coefficient (experimental).

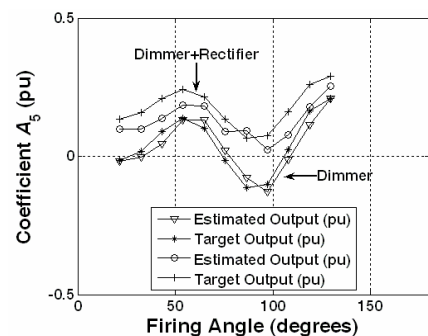


Fig. 15.  $A_5$  current coefficient (experimental).

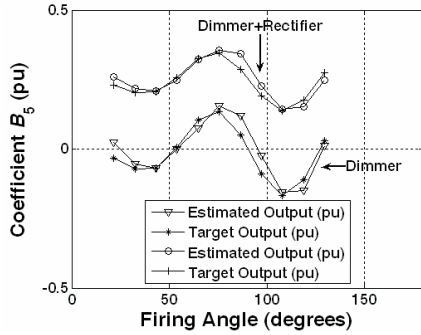


Fig. 16.  $B_5$  current coefficient (experimental).

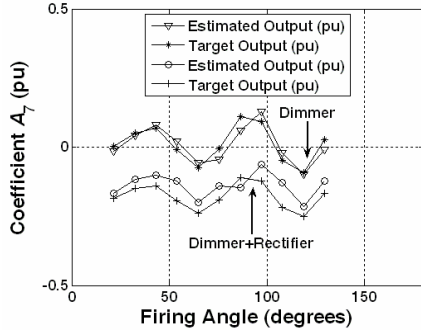


Fig. 17.  $A_7$  current coefficient (experimental).

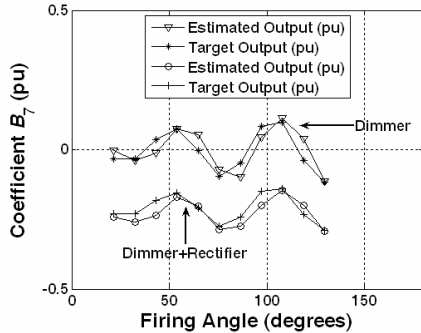


Fig. 18.  $B_7$  current coefficient (experimental).

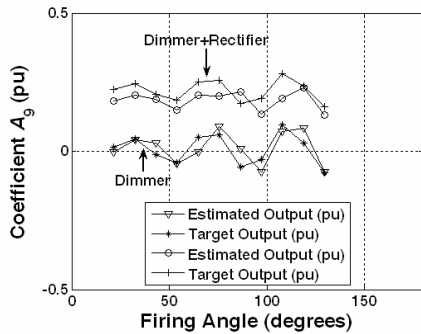


Fig. 19.  $A_9$  current coefficient (experimental).

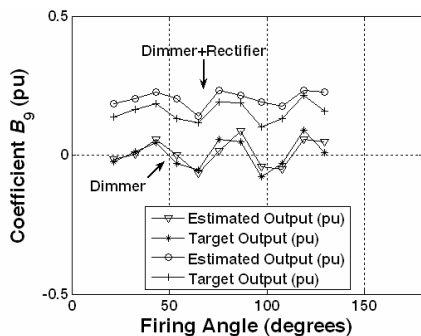


Fig. 20.  $B_9$  current coefficient (experimental).

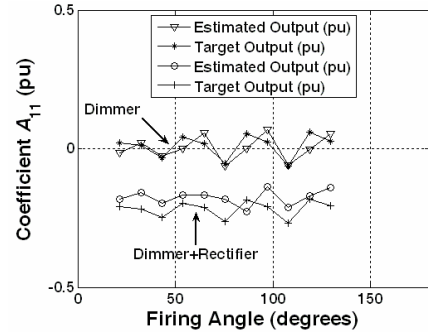


Fig. 21.  $A_{11}$  current coefficient (experimental).

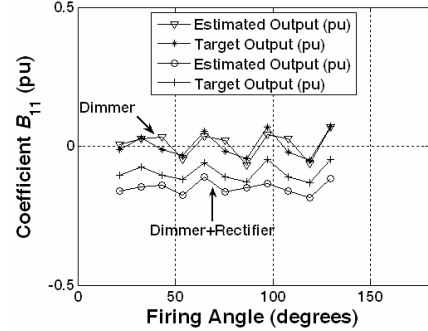


Fig. 22.  $B_{11}$  current coefficient (experimental).

Table I shows the amplitudes and phase angles of first six harmonic components of load currents (dimmer ( $\alpha=90^\circ$ ) and diode bridge rectifier) at PCC. They are calculated by (5) and (6) using the target and estimated coefficients. The estimated coefficients are obtained from ANN whereas the target coefficients are obtained from (8) and (9).

**TABLE I**  
**Current Amplitudes and Phases in the PCC**

$n$	Target Values		Estimated Values	
	$I_n$ (A)	$\theta_n$ (degrees)	$I_n$ (A)	$\theta_n$ (degrees)
1	2.07	-17.55	2.34	-15.00
3	0.93	150.52	0.88	155.08
5	0.74	12.80	0.89	14.33
7	0.66	-154.98	0.75	-152.16
9	0.63	44.97	0.73	47.79
11	0.56	-121.46	0.63	-119.64

The waveforms of Fig. 23 are generated from the harmonic components calculated with the coefficients of Table I. Fig. 23(a) shows the load current waveform ( $i_L(t)$ ) generated with target coefficient whereas Fig. 23(b) shows the waveform generated with estimated data. It is noticed that only the amplitude differs from each other.

### C. ANN and Truncated FFT Methods

The method based on ANN may be compared with Fast Fourier Transform (FFT) truncated at sixth harmonic component [16]. The FFT identifies the Discrete Fourier Transform (DFT) coefficients with better efficiency so that it enables the reconstruction of a discrete signal. The comparative analysis is achieved using a PQ parameter, i.e., THD. In Fig. 24, three THD curves which are generated from: (i) Truncated FFT (6 components); (ii) ANN (6 components); and (iii) FFT (ideal) are illustrated. It is verified that the results with ANN follow the truncated FFT curve behavior, which validates the proposed neural method.

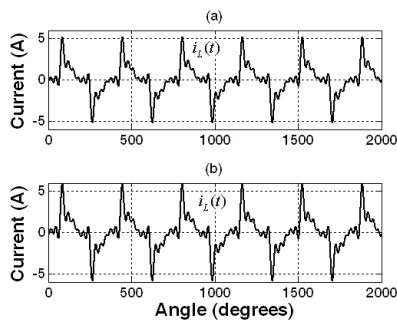


Fig. 23. Current with target data (a) and estimated data (b).

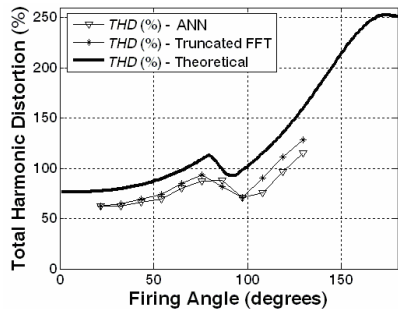


Fig. 24. ANN, truncated FFT and ideal FFT THD.

#### IV. CONCLUSION

In this paper, the amplitudes and phase of first six harmonic components of dimmer and diode bridge rectifier currents were calculated from the estimative of Fourier series coefficients ( $A_n$  e  $B_n$ ) after the theoretical and experimental characterization of those two widely applied nonlinear loads in single-phase electronic circuits. An alternative method based on ANN was developed for such coefficient estimative. The ANN method showed as an efficient solution for the harmonic current component determination both dimmer and the set of dimmer and diode bridge rectifier at PCC in half-cycle of current signal. The results obtained by neural methods were compared to those of truncated FFT, which demonstrate its applicability.

#### ACKNOWLEDGEMENT

The authors acknowledge the support received from CNPq (142128/2005-8 and 474290/2008-5) and FAPESP (06.56093-3 and 05.58404-3).

#### REFERENCES

[1] C. F. Nascimento, "Determination of the Current Harmonic Content Based on Artificial Neural Networks for Single-Phase Non-Linear Loads", Ph.D. Thesis (in Portuguese), Dept. Elect. Eng., University of São Paulo, São Carlos, SP, Brazil, 2007.

[2] C. F. Nascimento, A. A. Oliveira Júnior, A. Goedtel, I. N. Silva, M. Suetake, "A Neural Networks-Based Method for Single-Phase Harmonic Content Identification", in *Proc. of IECON*, pp. 2690-2695, 2008.

[3] J. A. Pomilio, and S. M. Bechmann, "Characterization and Compensation of Harmonics and Reactive Power of Residential and Commercial Loads", *Trans. Power Del.*, vol. 22, no. 2, pp. 1049-1055, April 2007.

[4] L. Sainz, J. Pedra, and J. J. Mesas, "Single-Phase Full-Wave Rectifier Study with Experimental Measurements", *Electric Power Systems Research*, vol. 77, no. 3-4, pp. 339-351, March 2007.

[5] L. Sainz, J. J. Mesas, and A. Ferrer, "Characterization of Non-Linear Load Behavior", *Electric Power Systems Research*, vol. 78, no. 10, pp. 1773-1783, Oct. 2008.

[6] H. Akagi, E. H. Watanabe, and M. Aredes, *Instantaneous Power Theory and Applications to Power Conditioning*, John Wiley, NJ, 2007.

[7] D. O. Abdeslam, P. Wira, J. Merckle, D. Flieller, and Y.-A. Chapuis, "A Unified Artificial Neural Network Architecture for Active Power Filters", *IEEE Trans. Ind. Electron.*, vol. 54, no.1, pp. 61-76, Feb. 2007.

[8] K.-K. Shyu, M. -J. Yang, Y.-M. Chen, and Y. -F. Lin, "Model Reference Adaptive Design for a Shunt Active-Power-Filter System", *IEEE Trans. Ind. Electron.*, vol. 55, no. 1, pp. 97-106, Jan. 2008.

[9] S. Mariethoz and A. C. Rufer, "Open Loop and Closed Loop Spectral Frequency Active Filtering", *IEEE Trans. Power Electron.*, vol. 17, no. 4, pp. 564-673, July 2002.

[10] M. Rukonuzzaman and M. Nakaoka, "Single-Phase Shunt Active Power Filter with Harmonic Detection", *IEE Proc. Electr. Power Appl.*, vol. 149, no. 5, pp. 343-350, Sept. 2002.

[11] B. K. Bose, "Neural Network Application in Power Electronic and Motor Drives-an Introduction and Perspective", *IEEE Trans. Ind. Electron.*, vol. 54, no. 1, pp. 14-33, Feb. 2007.

[12] H. Deng, R. Oruganti, and D. Srinivasan, "Neural Controller for UPS Inverters Based on B-Spline Network", *IEEE Trans. Ind. Electron.*, vol. 55, no. 2, pp. 899-909, Feb. 2008.

[13] C. A. Hudson, N. S. Lobo, and R. Krishnan, "Sensorless Control of Single Switch-Based Switched Reluctance Motor Drive Using Neural Network", *IEEE Trans. Ind. Electron.*, vol. 55, no. 1, pp. 321-329, Jan. 2008.

[14] S. Jung, and S. S. Kim, "Hardware Implementation of a Real-Time Neural Network Controller with a DSP and an FPGA for Nonlinear Systems", *IEEE Trans. Ind. Electron.*, vol. 54, no. 1, pp. 265-271, Feb. 2007.

[15] D. Zhang, and H. Li, "A Stochastic-Based FPGA Controller for an Induction Motor Drive with Integrated Neural Network Algorithms", *IEEE Trans. Ind. Electron.*, vol. 55, no. 2, pp. 551-561, Feb. 2008.

[16] J. G. Proakis and D. G. Manolakis, *Digital Signal Processing: principles, algorithms, and applications*, Prentice Hall, 3<sup>rd</sup> Edition, NJ, USA, 1996.

[17] R. W. Erickson, *Fundamentals of Power Electronics*, Chapman & Hall, NY, USA, 1997, pp. 541-652.

[18] S. Haykin, *Neural Networks: comprehensive foundation*, Englewood Cliffs, 2<sup>nd</sup> Edition, NJ, USA, 1999.